ELSEVIER

Physica A 239 (1997) 449–466

PHYSICA A

Shear modulus of fluids and solids

Siegfried Hess[a,*], Martin Kröger[a], William G. Hoover[b]

[a] *Institut für Theoretische Physik, Technische Universität Berlin, PN 7-1, Hardenbergstr. 36, D-10623 Berlin, Germany*

[b] *University of California at Davis/Livermore and Lawrence Livermore National Laboratory, Livermore, CA 94551-7808, USA*

Received 18 November 1996

Abstract

The shear modulus tensor, whose components are Voigt elastic moduli, is expressed as an N-particle average. The Born–Green and the fluctuation contributions are identified and, where possible, also expressed in terms of integrals over the pair-correlation function. Symmetry considerations are invoked for systems of spherical particles in both isotropic and cubic states. Results from molecular dynamics simulations are presented for particles with a purely repulsive Lennard–Jones interaction. Shear and bulk moduli are displayed graphically as functions of the density for fluid and cubic crystalline states. The shear modulus proves to be a good indicator for the fluid–solid phase transition.

1. Introduction

The fact that fluids do flow and solids do not is commonly attributed to the vanishing or non-vanishing of the shear modulus. Yet the Born–Green expression for the shear modulus is well defined [1] and yields non-zero results even for the fluid state [2]. This modulus characterizes the high frequency or short time response of a fluid just as does the "Maxwell shear modulus" in the visco-elastic Maxwell model. As is known from molecular dynamics (MD) computer simulations, the high-frequency shear modulus does not change dramatically at the fluid–solid phase transition, apart from effects associated with symmetry breaking [3]. The low-frequency shear modulus, referred to as "the shear modulus", is an indicator for the fluid or solid character of a system and can be computed from an equilibrium shear-free MD-simulation. The shear modulus is a sum of the Born–Green expresssion and "fluctuation terms" [4]. Though the fluctuation terms are only a small (but non-negligible) correction in the solid state,

* Corresponding author. E-mail: s.hess@physik.tu-berlin.de.

PII S0378-4371(97)00045-9

these same terms must cancel the Born–Green contribution to the shear modulus in the fluid state. Here we show this for a specific example, viz., for fluids and (cubic) solids composed of Lennard–Jones particles with the range of the force cut off at the minimum of the interaction potential (WCA potential). Firstly, however, we review the expressions needed to calculate the shear modulus tensor or the Voigt elastic moduli and discuss some general properties of these coefficients. Consequences of symmetry are exploited for systems with isotropic and cubic symmetry. Both the Voigt elastic modulus c_{44} and its orientationally averaged value G are referred to as "shear modulus"; in isotropic systems of spherical particles one has $c_{44} = G$. In a spirit similar to the present approach, the shear modulus has recently been calculated for thin films (between structured walls) which also undergo a fluid–solid phase transition [6].

This article is organized as follows. In Section 2, the pressure tensor and the shear modulus tensor are expressed as N-particle averages. The Voigt elastic moduli are components of the modulus tensor. The Born–Green contributions are averages of two-particle terms, the fluctuation contributions being squares of two-particle terms could also be written as averages of two-, three- and four-particle terms. The averages of the two-particle terms are also expressed as integrals over the pair correlation function. In Section 3, symmetry considerations are invoked for systems composed of spherical particles in states with isotropic and with cubic symmetry. Results of MD-simulations for WCA-particles are presented in Section 4. The pressure, Voigt elastic moduli, shear and bulk moduli and various contributions to these moduli are shown as functions of the density for fluid and for cubic crystalline (fcc and bcc) states. The total shear modulus does indeed vanish in the fluid due to the cancelation of the Born–Green and fluctuation contributions.

2. Basics: Pressure and shear moduli as averages

2.1. Pressure tensor

Consider a fluid composed of N molecules located at positions $\mathbf{r}^i$, $i = 1, 2, \ldots, N$ contained in a volume V. The total potential energy Φ is assumed to be the sum of pair potentials $\phi^{ij} = \phi(\mathbf{r}^{ij})$ acting between particles i and j, hence

$$\Phi = \sum_{i<j} \phi^{ij} = \sum_{i<j} \phi(\mathbf{r}^{ij}) . \tag{1}$$

Notice that a double summation both over i and j is meant here, $\mathbf{r}^{ij} = \mathbf{r}^i - \mathbf{r}^j$ is the relative position vector.

In thermal equilibrium, thermomechanical properties can be computed from the canonical distribution. The (potential contributions to the) pressure tensor and the elastic moduli can be inferred from the terms of first and second order in an expansion of the free energy with respect to the strain tensor $s_{\mu\nu}$. This expansion is obtained from the standard expression for the configurational Helmholtz free energy

$\beta F^{pot} = -\ln \int \exp(-\beta\Phi)\, dr^{\{N\}}$, $\beta = 1/(k_B T)$ with the position vectors $\mathbf{r}^i$ occurring in the potential displaced according to

$$r_\nu^i \to r_\nu^i + r_\mu^i s_{\mu\nu} . \tag{2}$$

Greek subscripts indicate cartesian components. The summation convention is used for them. The trace $s_{\mu\mu}$ is associated with a relative volume change. The antisymmetric and the symmetric traceless parts of $s_{\mu\nu}$ induce infinitesimal rotations and shear deformations, respectively.

The resulting expression for the potential part of the pressure tensor, which is equal to the stress tensor apart from a minus sign, is

$$V p_{\mu\nu}^{pot} = -\langle \Phi_{\mu\nu} \rangle, \quad \Phi_{\mu\nu} = -\sum_i r_\mu^i F_\nu^i = \sum_{i<j} \phi_{\mu\nu}^{ij} . \tag{3}$$

The bracket $\langle \ldots \rangle$ indicates an N-particle average, $\mathbf{F}^i$ is the force acting on particle i and the second rank tensor $\phi_{\mu\nu}^{ij}$ is defined by

$$\phi_{\mu\nu}^{ij} = \phi_{\mu\nu}(\mathbf{r}^{ij}), \qquad \phi_{\mu\nu}(\mathbf{r}) = r_\mu \hat{c}_\nu \phi(\mathbf{r}) , \tag{4}$$

where $\hat{c}_\nu$ stands for the partial derivative with respect to r_ν.

The scalar pressure P is the trace of the total pressure tensor divided by D, the spatial dimension: $P = (1/D) p_{\mu\mu}$. In addition to the obvious value $D = 3$, the case $D = 2$ deserves some attention, not only in view of model calculations [17] but also due to its applicability to thin film systems [6]. In general, P is the sum of the kinetic part nk_BT (n is the particle number density) and the potential contribution $p_{pot} = (1/D) p_{\mu\mu}^{pot}$. The symmetric traceless part of $p_{\mu\nu}$ is associated with the shear stress. The antisymmetric part of $p_{\mu\nu}$ vanishes for particles with spherical interaction.

The quantity $\Phi_{\mu\nu}$ of (3) being a sum of two-particle variables, the average can also be expressed as an integral over the pair-correlation function $g(\mathbf{r})$:

$$p_{\mu\nu}^{pot} = -\frac{1}{2} n^2 \int \phi_{\mu\nu}(\mathbf{r}) g(\mathbf{r})\, d^D r , \tag{5}$$

where $n = N/V$ is the number density. With the pair-correlation function written as $g(\mathbf{r}) = \chi(\mathbf{r}) \exp(-\beta\phi(\mathbf{r}))$ where $\phi(\mathbf{r})$ is the pair potential function, (5) is equivalent to

$$p_{\mu\nu}^{pot} = \frac{1}{2} n^2 k_B T \int \chi(\mathbf{r}) r_\mu \hat{c}_\nu \exp(-\beta\phi(\mathbf{r}))\, d^D r , \tag{6}$$

and, after an integration by parts, to

$$p_{\mu\nu}^{pot} = \frac{1}{2} n^2 k_B T \int (1 - \exp(-\beta\phi(\mathbf{r}))(\chi(\mathbf{r})\delta_{\mu\nu} + r_\mu \hat{c}_\nu \chi(\mathbf{r}))\, d^D r . \tag{7}$$

Here $\delta_{\mu\nu}$ is the unit tensor. These expressions are standard, in particular, Eq. (6) is used for hard spheres, and the second virial coefficient can be inferred from Eq. (7) with the low-density limit $\chi = 1$. These formulae are listed here for comparison with the equations needed to compute the elastic moduli.

2.2. Elastic modulus tensor

Let $\sigma_{\mu\nu} = -(p_{\mu\nu}^{pot,def} - p_{\mu\nu}^{pot,0}) = -\delta p_{\mu\nu}^{pot} = \delta(V^{-1}\langle\Phi_{\mu\nu}\rangle)$ be the part of the stress tensor which is the (negative) difference between the (potential contribution to the) pressure tensor $p_{\mu\nu}^{pot,def}$ in the deformed (strained) state and its corresponding value $p_{\mu\nu}^{pot,0}$ in the unstrained state. The linear relation between $\sigma_{\mu\nu}$ and the strain tensor $s_{\lambda\kappa}$ defines the elastic modulus tensor $G_{\ldots\ldots}$:

$$\sigma_{\mu\nu} = G_{\mu\nu,\lambda\kappa} s_{\lambda\kappa} , \tag{8}$$

with

$$VG_{\mu\nu,\lambda\kappa} = \langle\Phi_{\mu\nu,\lambda\kappa}\rangle_0 + Vp_{pot}\delta_{\mu\nu}\delta_{\lambda\kappa} - \beta(\langle\Phi_{\mu\nu}\Phi_{\lambda\kappa}\rangle_0 - \langle\Phi_{\mu\nu}\rangle_0\langle\Phi_{\lambda\kappa}\rangle_0) . \tag{9}$$

The second term on the r.h.s. of (9) stems from the deformation-induced variation δV of the volume V in (8), $\delta V/V = s_{\lambda\lambda}$ and $-\langle\Phi_{\mu\nu}\rangle_0 = Vp_{pot}\delta_{\mu\nu}$ were used, where p_{pot} is the potential part of the pressure P. The other terms of (9) follow from the variation of $\langle\Phi_{\mu\nu}\rangle$. The subscript "0" as in $\langle\ldots\rangle_0$ indicates that the average is to be evaluated in the unstrained state. The first term in the expression for the elastic modulus tensor $G_{\mu\nu,\lambda\kappa}$ involves the fourth rank tensor

$$\Phi_{\mu\nu,\lambda\kappa} = \sum_{i<j} \phi_{\mu\nu,\lambda\kappa}^{ij} , \tag{10}$$

with

$$\phi_{\mu\nu,\lambda\kappa}^{ij} = \phi_{\mu\nu,\lambda\kappa}(\mathbf{r}^{ij}), \quad \phi_{\mu\nu,\lambda\kappa}(\mathbf{r}) = r_\mu \hat{c}_\nu r_\lambda \hat{c}_\kappa \phi(\mathbf{r}) = \phi_{\mu\kappa}\delta_{\nu\lambda} + r_\mu r_\lambda \hat{c}_\nu \hat{c}_\kappa \phi(\mathbf{r}) . \tag{11}$$

The first and the second terms of (9) correspond to the *Born–Green* expression for the elastic modulus tensor. The remaining terms with the factor β are referred to as *fluctuation* contributions.

As a side remark, it should be mentioned that the fluctuation contribution to the shear modulus tensor is the negative of the "initial value" at time $t = 0$ of the time correlation function tensor

$$\mathscr{C}_{\mu\nu,\lambda\kappa}(t) = V^{-1}\beta\langle\tilde{\Phi}_{\mu\nu}(t)\tilde{\Phi}_{\lambda\kappa}(0)\rangle_0, \quad \tilde{\Phi}_{\mu\nu} = \Phi_{\mu\nu} - \langle\Phi_{\mu\nu}\rangle_0 , \tag{12}$$

which is linked to the potential contribution to the viscosity tensor $\eta_{\mu\nu,\lambda\kappa}$ by the Green–Kubo relation

$$\eta_{\mu\nu,\lambda\kappa} = \int_0^\infty \mathscr{C}_{\mu\nu,\lambda\kappa}(t)\, dt . \tag{13}$$

In the following, systems composed of spherical particles are considered. Then the interaction potential depends on $\mathbf{r}$ via $r = |\mathbf{r}|$ and one has, with the prime indicating

the differentiation with respect to r,

$$\phi_{\mu\nu}(\mathbf{r}) = r_\mu r_\nu r^{-1}\phi' , \tag{14}$$

$$\phi_{\mu\nu,\lambda\kappa}(\mathbf{r}) = (r_\mu r_\kappa \delta_{\nu\lambda} + r_\mu r_\lambda \delta_{\nu\kappa}) r^{-1}\phi' + r_\mu r_\nu r_\lambda r_\kappa r^{-1}(r^{-1}\phi')' . \tag{15}$$

These relations are used next for the Voigt elastic modulus c_{44}, which characterizes the shear behavior.

2.3. Voigt moduli, shear modulus

The shear behavior can be inferred from the elastic coefficient $G_{yx,yx}$, which links the yx component of the stress tensor with the yx component of the deformation tensor corresponding to a displacement $x \to x + ys_{yx}$. In the Voigt notation, one writes for the shear modulus $c_{44} = G_{yx,yx}$. The standard symmetrization according to $c_{44} = (G_{yx,yx} + G_{yx,xy} + G_{xy,yx} + G_{xy,xy})/4$ is not essential for particles with central interaction. With the obvious decomposition $c_{44} = c_{44}^{BG} + c_{44}^{flct}$ into *Born–Green* and *fluctuation* contributions, one obtains

$$Vc_{44}^{BG} = \left\langle \sum_{i<j} (y^2 r^{-1}\phi')^{ij} \right\rangle_0 + \left\langle \sum_{i<j} (x^2 y^2 r^{-1}(r^{-1}\phi')')^{ij} \right\rangle_0 , \tag{16}$$

$$Vc_{44}^{flct} = -\beta \left[\left\langle \left(\sum_{i<j} (xyr^{-1}\phi')^{ij} \right)^2 \right\rangle_0 - \left(\left\langle \sum_{i<j} (xyr^{-1}\phi')^{ij} \right\rangle_0 \right)^2 \right] . \tag{17}$$

One has $\langle \sum_{i<j} (xyr^{-1}\phi')^{ij} \rangle_0 = 0$ for a system with isotropic or cubic symmetry. Notice that the first term of (16) is $-Vp_{yy}^{pot}$ which, in turn, is equal to $-Vp_{pot}$ for a system with an isotropic pressure tensor in the unstrained state. Then the sum of (16) and (17) becomes equivalent to

$$c_{44} = c_{44}^{BG} + c_{44}^{flct} = c_{44}^0 - P , \tag{18}$$

where c_{44}^0 is expression for the shear modulus derived in [4] for the case $P = nk_BT + p_{pot} = 0$. The full expression for $P \neq 0$ has already been stated in [5].

For an isotropic system, c_{44} is equal to the orientationally averaged shear modulus G. Its *Born–Green* part is given by

$$G^{GB} = V^{-1}c(D) \left\langle \sum_{i<j} (r^3(r^{-1}\phi')')^{ij} \right\rangle_0 - p_{pot} . \tag{19}$$

The numerical factor $c(D)$ with $c(3) = \frac{1}{15}$ and $c(2) = \frac{1}{8}$ is the orientational average of $x^2y^2r^{-4}$ in a D-dimensional isotropic system. For $D = 3$, Eq. (19) is equivalent to

$$G^{GB} = \frac{1}{15V} \left\langle \sum_{i<j} (r^{-2}(r^4\phi')')^{ij} \right\rangle_0 . \tag{20}$$

Similarly, for $D=2$, where V stands for an area, one has

$$G^{GB}=\frac{1}{8V}\left\langle \sum_{i<j}(r^{-1}(r^3\phi')')^{ij}\right\rangle_0 . \tag{21}$$

Other Voigt moduli, such as $c_{11}=G_{xx,xx}$ and $c_{12}=G_{xx,yy}$ can also be inferred from (9) with (11)–(15). The relations of these moduli to the shear and the bulk modulus will be stated later in connection with general symmetry considerations.

It should be mentioned that the total elastic modulus tensor also contains the kinetic contribution $nk_BT\,\delta_{\mu\nu}\delta_{\lambda\kappa}$. This does not affect the shear modulus but both c_{11} and c_{12} possess a kinetic contribution nk_BT. The total moduli c_{11}^{total} and c_{12}^{total} are related to the c_{11} and c_{12} used here and to the moduli for zero pressure c_{11}^0 and c_{12}^0 of [4] by

$$c_{11}^{total}=c_{11}+nk_BT=c_{11}^0-P\,, \tag{22}$$

$$c_{12}^{total}=c_{12}+nk_BT=c_{12}^0+P\,. \tag{23}$$

2.4. Pair contributions to the elastic moduli

The Born–Green contribution $G^{BG}_{\mu\nu,\lambda\kappa}$ can readily be expressed as an intergral over the pair correlation function

$$G^{BG}_{\mu\nu,\lambda\kappa}=\frac{1}{2}n^2\int \phi_{\mu\nu,\lambda\kappa}(\mathbf{r})g(\mathbf{r})\,d^3r+p_{pot}\delta_{\mu\nu}\delta_{\lambda\kappa}\,, \tag{24}$$

with $p_{pot}=-(1/2D)n^2\int r\phi' g(\mathbf{r})\,d^Dr$. The fluctuation contributions, on the other hand, involve also three- and four-particle terms. The quantity

$$\Psi_{\mu\nu,\lambda\kappa}=\sum_{i<j}\phi^{ij}_{\mu\nu}\phi^{ij}_{\lambda\kappa}\,, \tag{25}$$

is the part of $\Phi_{\mu\nu}\Phi_{\lambda\kappa}$ that involves two-particle terms. Thus, e.g., the pair contribution to the fluctuation part of c_{44} is

$$Vc_{44}^{flct,pair}=-\beta\langle\Psi_{yx,yx}\rangle_0\,. \tag{26}$$

The pair contribution to the modulus c_{44} is $c_{44}^{pair}=c_{44}^{BG}+c_{44}^{flct,pair}$. It can be expressed as an integral over the pair correlation function $g(\mathbf{r})$, viz.,

$$Vc_{44}^{pair}=\frac{1}{2}n^2\int g(\mathbf{r})(y\partial_x\phi_{yx}-\beta\phi_{yx}\phi_{yx})\,d^Dr\,. \tag{27}$$

Here, x and y stand for r_x and r_y. Use of $g(\mathbf{r})=\chi(\mathbf{r})\exp(-\beta\phi(\mathbf{r}))$ and an integration by parts leads to

$$c_{44}^{pair}=-\frac{1}{2}n^2\int g(\mathbf{r})\phi_{yx}y\partial_x\ln\chi(\mathbf{r})\,d^Dr\,, \tag{28}$$

and

$$c_{44}^{pair}=\frac{1}{2}n^2k_BT\int(y\partial_x\chi(\mathbf{r}))y\partial_x\exp(-\beta\phi(\mathbf{r})\,d^Dr\,. \tag{29}$$

Notice that the expression (29) is well defined also for a fluid of hard spheres or disks. For a three-dimensional system of spherical particles in an isotropic state, the above expressions for c_{44}^{pair} reduce to

$$G^{pair} = -\frac{1}{30}n^2 \int g(r) r^2 \phi'(\ln \chi(r))' \, d^3r \,, \tag{30}$$

or

$$G^{pair} = \frac{1}{30}n^2 k_B T \int r^2 \chi(r)' (\exp(-\beta\phi(r)))' \, d^3r \,. \tag{31}$$

Clearly, G^{pair} vanishes in the dilute density limit where $\chi(r) = 1$. This is in contradistinction to the corresponding expression

$$G^{BG} = \frac{1}{30}n^2 k_B T \int r^{-2} (r^4 \phi')' g(r) \, d^3r \tag{32}$$

for the Born–Green shear modulus; cf. (20).

3. Symmetry considerations

3.1. Spherical particles in an isotropic state

For an isotropic system composed of spherical particles, the bulk modulus B and the shear modulus G characterize the elastic properties. Then Eq. (8) reduces to

$$\sigma_{\mu\nu} = B\delta_{\mu\nu} s_{\lambda\lambda} + 2G\overline{s_{\mu\nu}} \,, \tag{33}$$

where the symbol $\overline{\ldots}$ indicates the symmetric traceless part of a tensor, e.g.

$$\overline{s_{\mu\nu}} = \tfrac{1}{2}(s_{\mu\nu} + s_{\nu\mu}) - \tfrac{1}{3} s_{\lambda\lambda} \delta_{\mu\nu} \,. \tag{34}$$

Here we restrict our considerations to the three-dimensional case. Isotropy implies that the elastic modulus tensor can be written as

$$G_{\mu\nu,\lambda\kappa} = B\delta_{\mu\nu}\delta_{\lambda\kappa} + 2G\Delta_{\mu\nu,\lambda\kappa} \,, \tag{35}$$

with the isotropic tensor of rank four defined by

$$\Delta_{\mu\nu,\lambda\kappa} = \tfrac{1}{2}(\delta_{\mu\lambda}\delta_{\nu\kappa} + \delta_{\mu\kappa}\delta_{\nu\lambda}) - \tfrac{1}{3}\delta_{\mu\nu}\delta_{\lambda\kappa} \,. \tag{36}$$

The moduli B and G can be inferred from the elastic modulus tensor according to

$$B = \tfrac{1}{9} G_{\mu\mu,\lambda\lambda} \,, \tag{37}$$

$$G = \tfrac{1}{10} \Delta_{\mu\nu,\lambda\kappa} G_{\mu\nu,\lambda\kappa} \,. \tag{38}$$

These quantities are sums of Born–Green and fluctuation contributions. Previous expressions, e.g. for G^{BG}, cf. Eq. (20), can be recovered from (38) with (9).

Furthermore, the total bulk modulus has the kinetic contribution nk_BT in addition to (37). The definitions (37) and (38) for B and G can also be used for a system with cubic symmetry.

The relation between the Voigt moduli $c_{11} = G_{xx,xx}$, $c_{12} = G_{xx,yy}$ and the elastic moduli B, G in an isotropic state can by inferred from the corresponding relations for a system with cubic symmetry when an additional cubic modulus G_c is put equal to zero. These more general relations are presented next.

3.2. Spherical particles in a cubic state

For a system with cubic symmetry and with the cubic axes parallel to the coordinate axes, one has

$$\begin{aligned} c_{11} = c_{22} = c_{33} &= B + \tfrac{4}{3}G + \tfrac{4}{5}G_c\,, \\ c_{12} = c_{23} = c_{31} &= B - \tfrac{2}{3}G - \tfrac{2}{5}G_c\,, \\ c_{44} = c_{55} = c_{66} &= G - \tfrac{2}{5}G_c\,, \end{aligned} \tag{39}$$

or, equivalently

$$B = \tfrac{1}{3}(c_{11} + 2c_{12}), \qquad G = \tfrac{1}{5}(c_{11} - c_{12} + 3c_{44}) \tag{40}$$

and

$$G_c = \tfrac{1}{2}(c_{11} - c_{12} - 2c_{44})\,. \tag{41}$$

The shear modulus for a shear deformation in the xy-plane rotated by an angle of 45° from these directions is

$$\tilde{c}_{44} = \tfrac{1}{2}(c_{11} - c_{12}) = G + \tfrac{3}{5}G_c\,. \tag{42}$$

The cubic modulus G_c, which is the difference between $\tilde{c}_{44}$ and c_{44}, vanishes in an isotropic state. Then one has, as mentioned before, $c_{44} = G$, and $\tilde{c}_{44} = c_{44}$.

Microscopic expressions for the moduli B, G and G_c can now be inferred from the relations given above since the Voigt moduli are components of the shear modulus tensor (9). The Born–Green contributions to these coefficients are

$$B^{BG} = \tfrac{5}{3}G^{BG} + 2p_{pot}\,, \tag{43}$$

with G^{BG} given by (20), and

$$G_c^{GB} = \frac{5}{12V}\left\langle \sum_{i<j} (H(\mathbf{r})r^{-1}(r^{-1}\phi')')^{ij} \right\rangle_0, \quad H(\mathbf{r}) = x^4 + y^4 + z^4 - \tfrac{3}{5}r^4\,. \tag{44}$$

The quantity $H(\mathbf{r})$ is a cubic harmonic [7,8]. With the abbreviations

$$\Phi_{iso} = \frac{1}{3}\sum_{i<j}(r\phi')^{ij}, \quad \Phi_{+} = \sum_{i<j}(xyr^{-1}\phi')^{ij},$$

$$\Phi_{-} = \frac{1}{2}\sum_{i<j}((x^2-y^2)r^{-1}\phi')^{ij}, \tag{45}$$

the fluctuation contributions to the elastic moduli are given by

$$VB^{flct} = -\beta[\langle\Phi_{iso}^2\rangle_0 - (\langle\Phi_{iso}\rangle_0)^2], \tag{46}$$

$$VG^{flct} = -\frac{1}{5}\beta[3\langle\Phi_{+}^2\rangle_0 + 2\langle\Phi_{-}^2\rangle_0], \tag{47}$$

$$VG_c^{flct} = -\beta[\langle\Phi_{-}^2\rangle_0 - \langle\Phi_{+}^2\rangle_0]. \tag{48}$$

Of course, these Born–Green and fluctuation contributions to the moduli have to be added, e.g. $G = G^{GB} + G^{flct}$.

In a cubic state, the relation corresponding to (35) is

$$G_{\mu\nu,\lambda\kappa} = B\delta_{\mu\nu}\delta_{\lambda\kappa} + 2G\Delta_{\mu\nu,\lambda\kappa} + 2G_c H_{\mu\nu\lambda\kappa}. \tag{49}$$

Here

$$H_{\mu\nu\lambda\kappa} = \sum_{i=1}^{3} e_\mu^i e_\nu^i e_\lambda^i e_\kappa^i - \frac{1}{5}(\delta_{\mu\nu}\delta_{\lambda\kappa} + \delta_{\mu\lambda}\delta_{\nu\kappa} + \delta_{\mu\kappa}\delta_{\nu\lambda}) \tag{50}$$

is an irreducible tensor of rank four with cubic symmetry. The unit vectors parallel to the cubic axes are denoted by $\mathbf{e}^i$, $i=1,2,3$. Notice that $H(\mathbf{r}) = H_{\mu\nu\lambda\kappa}r_\mu r_\nu r_\lambda r_\kappa$. Furthermore, due to $H_{\mu\nu\lambda\kappa}\delta_{\mu\nu}\delta_{\lambda\kappa} = 0$, $H_{\mu\nu\lambda\kappa}\Delta_{\mu\nu,\lambda\kappa} = 0$, and $H_{\mu\nu\lambda\kappa}H_{\mu\nu\lambda\kappa} = \frac{6}{5}$, relations (37) and (38) still apply in the cubic state, and the modulus G_c is also given by

$$G_c = \tfrac{5}{12}H_{\mu\nu\lambda\kappa}G_{\mu\nu,\lambda\kappa}. \tag{51}$$

In the following, results from MD-simulations will be presented where the N-particle averages over a canonical distribution considered so far are replaced by time averages.

4. Molecular dynamics results

4.1. The model system

Molecular dynamics simulations were performed for a simple model system with both fluid and solid phases. The particles interact via the purely repulsive WCA-potential,

$$\phi(r) = 4(r^{-12} - r^{-6}) + 1, \quad r < r_{cut} = 2^{1/6}, \tag{52}$$

and $\phi(r) = 0$ for $r > r_{cut}$. This is essentially the Lennard–Jones (LJ) potential cut off in its minimum at r_{cut}. Here and in the following, all physical quantities are in the standard

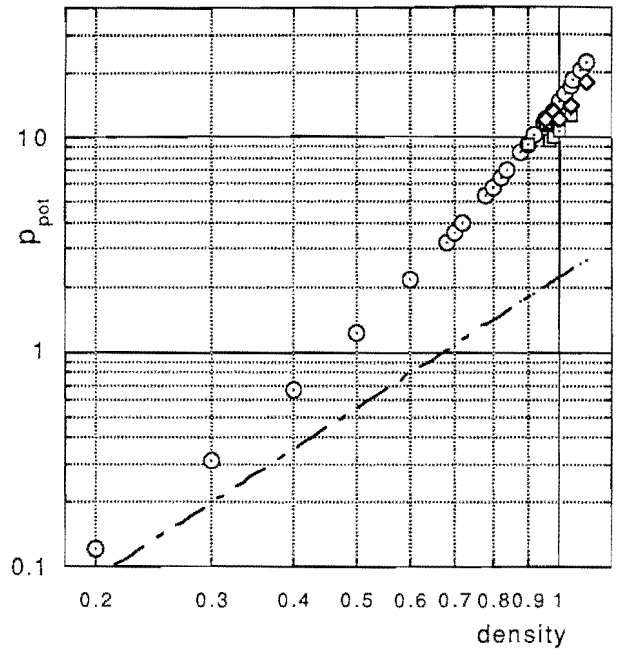

Fig. 1. Double logarithmic plot of the potential contribution to the pressure p_{pot} as a function of the number density n (in Lennard–Jones units). Circles, squares and diamonds refer to data for isotropic, fcc and bcc states. The dashed line indicates the low-density limit with the slope determined by the second virial coefficient.

LJ-units of [4–14]. Simulations with constant temperature $T=1$ and constant number densities $n=N/V$ in the range $n=0.1,\ldots,1.1$ were performed for $N=1000$, 1024 and 2048 particles where the initial positions were *simple cubic*, *bcc* and *fcc* lattice sites. The equations of motion were integrated with the velocity Verlet algorithm with the time step $\delta t=0.002$. A cubic simulation box with volume V and periodic boundary conditions were used. The temperature was kept constant by rescaling the magnitude of the particle velocities. The system was aged (for 25 000 or more time steps) before the data were extracted as time averages over 25 000 to 100 000 time steps. Aged states were also subjected to (small) density changes in order to obtain data for neighboring densities. Details on the method of molecular dynamics (equilibrium and non-equilibrium: MD and NEMD) simulation are found in the literature [9–15].

The potential contribution to the pressure is shown in Fig. 1 as a function of the density n in a double logarithmic plot. Data for simulations with 1000, 1024 and 2048 particles corresponding to simple cubic, fcc and bcc initial states are marked as circles, squares and diamonds, respectively. The dashed line indicates the low-density limit with the slope determined by the second virial coefficient.

The simple cubic lattice is highly unstable. Thus, the circles show data for aged systems which are in an isotropic state. The situation is different when the initial state is of fcc or bcc type; see Fig. 2, where p_{pot} is displayed in a linear plot for the higher densities. For densities $n\geqslant 0.97$, the "square pressures" are smaller than the corresponding values in the isotropic state (circles), i.e. the fcc state is stable.

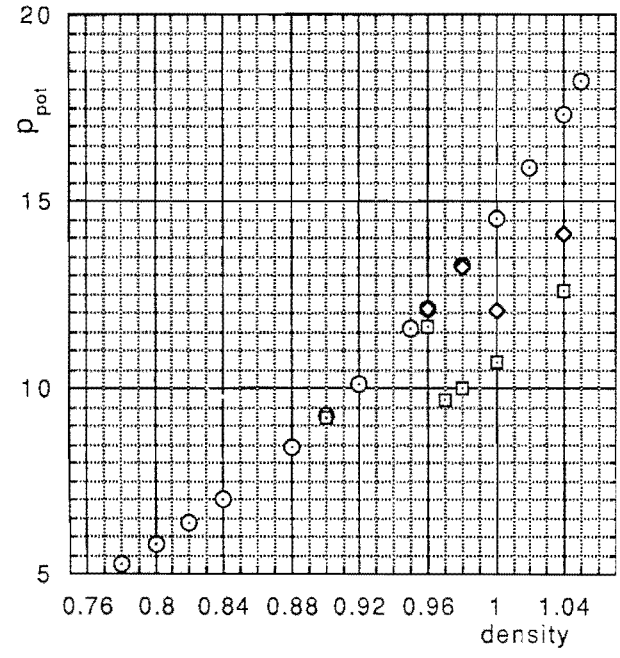

Fig. 2. Linear plot of the potential contribution to the pressure p_{pot} as function of the density n (in Lennard–Jones units). Circles, squares and diamonds refer to data for simulations where the intial state were simple cubic, fcc and bcc states, resp.

For $n \leqslant 0.96$, on the other hand, the initial fcc crystal melts as indicated by the squares approaching the circles. The pressure data for the (initial) bcc state (diamonds) indicate that the (metastable) bcc crystal melts at densities below $n = 1$. Instabilities of the isotropic and of the bcc states at densities higher than $n = 1.1$ are not studied here.

The number densities n used here can be converted to packing fractions nv_{eff} where v_{eff} is the effective volume of a particle. With v_{eff} identified with one-quarter of the second virial coefficient, one has $v_{eff} = 0.551$ for $T = 1$. Then the number densities 0.96 and 0.97 where the system was found to be in fluid and in the fcc states correspond to packing fractions of 0.529 and 0.534, respectively, which are close to the value where the hard sphere crystal melts [16].

In short, the data for the pressure show that we have well-defined samples of systems in isotropic and in cubic (crystalline) states for which also the elastic moduli can and have been computed. Results are presented next.

4.2. *Shear modulus* c_{44}

The Born–Green (filled circles) and the negative of the fluctuation (open circles) contributions to the elastic modulus, i.e. the quantities c_{44}^{BG} and $-c_{44}^{fluct}$ as evaluated according to Eqs. (16) and (17) are plotted as functions of the density in Fig. 3. All data shown are for the isotropic state. The dashed line is the low-density limit of the shear modulus G calculated from (32) with the pair correlation function

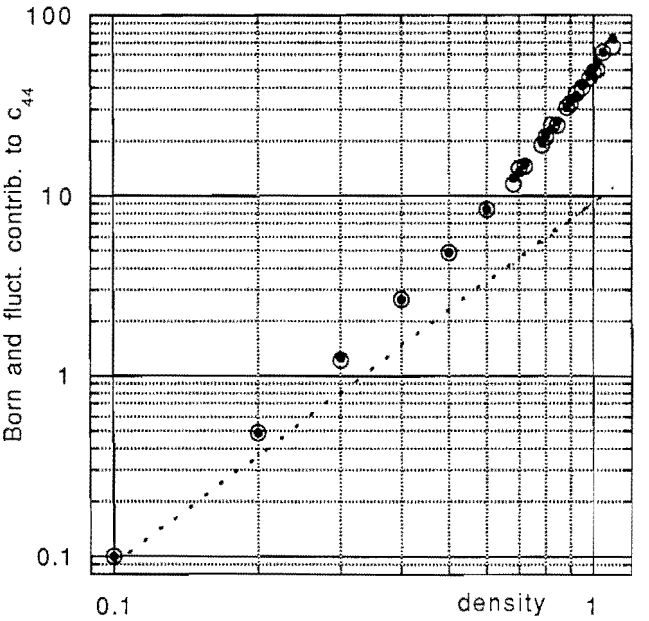

Fig. 3. The Born–Green (filled circles) and the fluctuation contributions (open circles) to the elastic modulus c_{44} as function of the density n. The dashed line marks the low-density limit.

approximated by $g = \exp(-\beta\phi)$. In the isotropic state, the Born–Green contribution to the orientationally averaged shear modulus G evaluated according to (20) cannot be distinguished from c_{44}^{BG} on the scale of the figure, thus these data are not shown. The fact that the "BG" values and the "flct" values practically coincide indicates that the Born–Green and fluctuation contributions to the shear modulus c_{44} approximately cancel each other. This is no longer the case at higher densities and in the cubic crystalline states.

In Fig. 4 the Born–Green (filled symbols) and the negative of the fluctuation (open symbols) contributions to the elastic modulus, i.e. the quantities c_{44}^{BG} and $-c_{44}^{flct}$, cf. Eqs. (16) and (17) are plotted for the higher densities considered here. Again, circles indicate data for an isotropic state, the squares and diamonds are for simulations which started from fcc and bcc lattices but may not necessarily be in a state of this symmetry. Clearly, at high densities, the open symbols lie below their corresponding filled ones, which means the fluctuation contributions are smaller in magnitude than the Born–Green contribution and a finite (positive) shear modulus results.

In Fig. 5 the elastic modulus $c_{44} = c_{44}^{BG} + c_{44}^{flct}$ is displayed for the same data as used in Fig. 4. The shear modulus is positive, indicating a solid phase, at the higher densities and it vanishes, within the computational accuracy, at the lower densities, where the system is fluid. Notice that c_{44} increases approximately linearly with the density in the cubic states. Such a behavior is also seen in experiments with colloidal crystals [18] although there the interaction is of screened Coulomb type rather than the WCA potential used here.

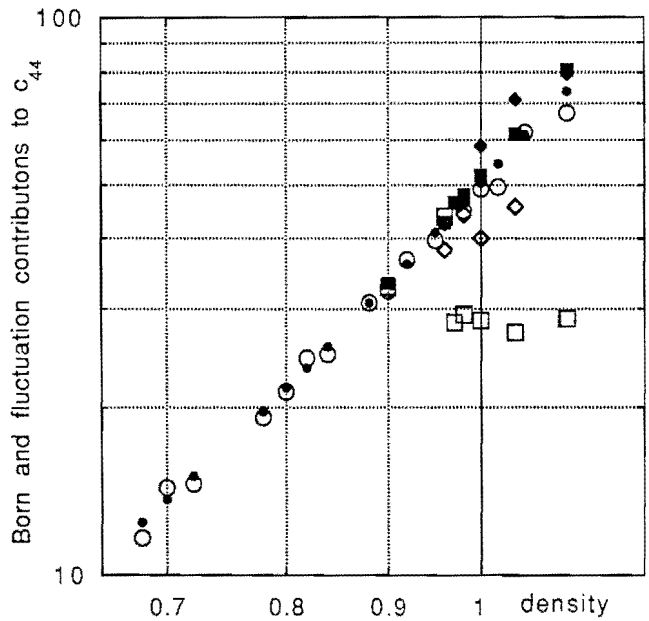

Fig. 4. The Born–Green (filled symbols) and the fluctuation contributions (open symbols) to the elastic modulus c_{44} as function of the density n for higher densities. Circles, squares and diamonds refer to data for simulations of isotropic, fcc and bcc states.

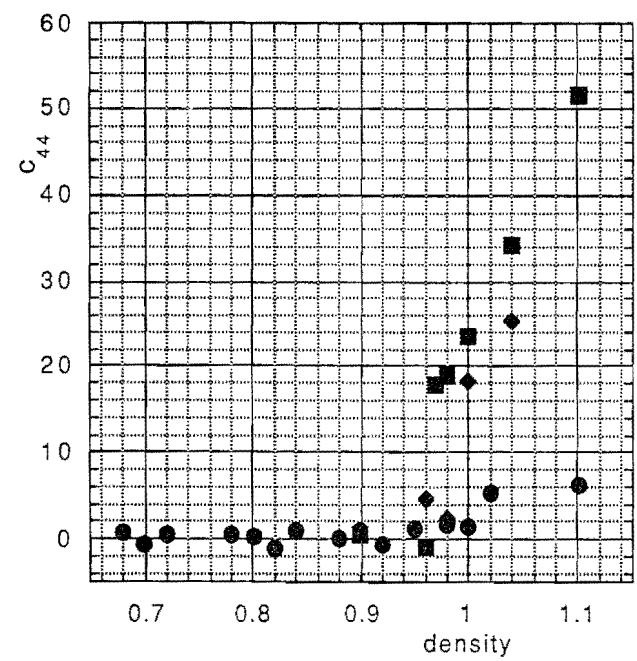

Fig. 5. The elastic modulus c_{44} as a function of the density n for higher densities. Circles, squares and diamonds refer to data for simulations of isotropic, fcc and bcc states, respectively.

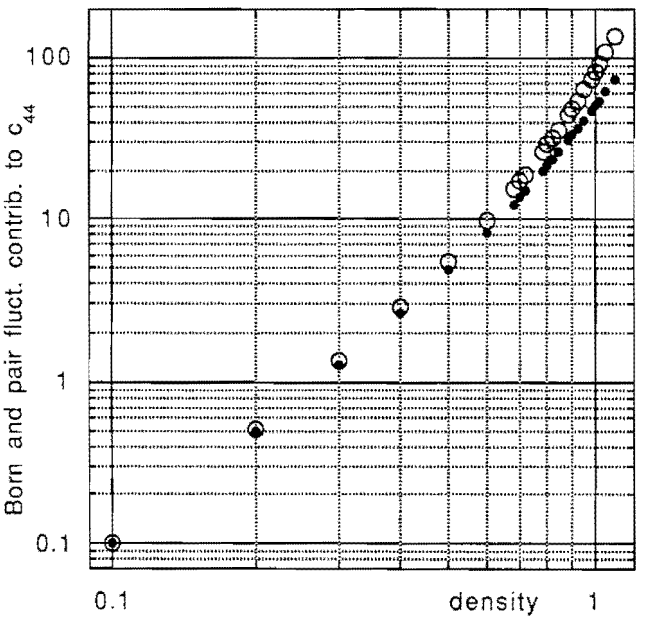

Fig. 6. The Born–Green modulus c_{44}^{BG} (filled circles) and the negative pair contribution $-c_{44}^{flct,pair}$ (open circles) to the fluctuation elastic modulus c_{44}^{flct} as functions of the density for the isotropic state (fluid for $n \lessapprox 1$).

4.3. Pair contribution to the fluctuation part of the shear modulus

In Fig. 6 the negative pair contribution $-c_{44}^{flct,pair}$ (open circles) to the fluctuation elastic modulus c_{44}^{flct} as calculated according to (26) with (25) is compared with the Born–Green modulus c_{44}^{BG} (filled circles), which is essentially equal to $-c_{44}^{flct}$. All data are for the isotropic state which is fluid for $n \lessapprox 1$. Here, the difference between the open and filled circles is a measure of the importance the three- and four-particle terms in Eq. (17). As expected, these terms are negligible at low densities $n < 0.4$. At higher densities, however, the two-particle contributions overestimate the magnitude of the fluctuation modulus: $-c_{44}^{flct,pair} > -c_{44}^{flct}$.

4.4. Bulk modulus in the isotropic state

In the simulations also the (isothermal) bulk modulus $B = B^{BG} + B^{flct}$ was calculated using the relations (43) and (46). In Fig. 7 the filled circles represent such values for B in the fluid state. The triangles in between indicate the values for the bulk modulus calculated according to $\frac{1}{2}(n_l + n_r)(p_r - p_l)/(n_r - n_l)$, where $p_{l,r}$ are the potential contribution to the pressure computed at the densities n_l and n_r to the left and right of the intermediate densities. The two sets of data agree well within the computational accuracy.

In addition to the isothermal (isokinetic) simulations discussed here, also some simulations at constant total energy were performed. At state points not too close to a

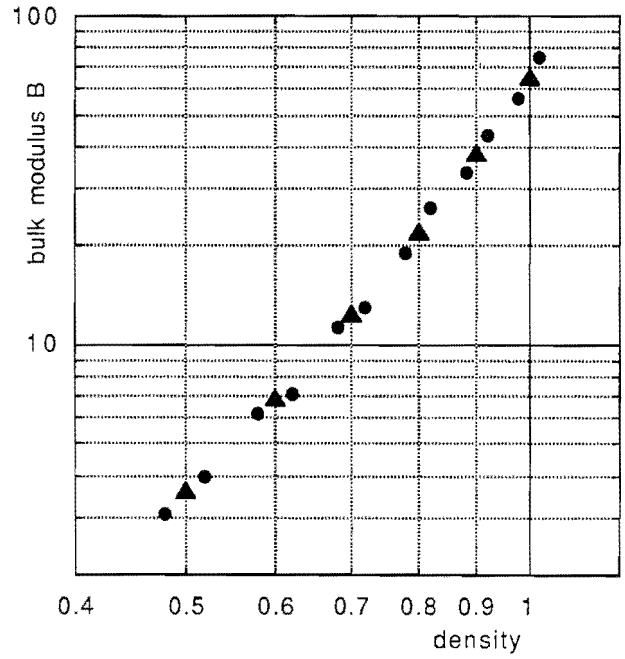

Fig. 7. The bulk modulus B as a function of the density n for the fluid state. The filled circles show the values computed according to $B = B^{BG} + B^{flct}$ as given in the text; the triangles in between are the values inferred from the ratio of the pressure and density differences.

phase transition where the temperature of the isoenergetic simulations did not deviate from the corresponding isokinetic ones by more than about 1%, the potential contribution to the pressure and the Born–Green contributions to the elastic moduli are practically identical for the isothermal and for the isoenergetic simulations. This is not the case for the fluctuation contributions. These differences are small for G and G_c but considerable for B in the sense that the magnitude of the fluctuations is smaller in the isoenergetic case. Thus, the difference between the adiabatic and the isothermal values of the bulk modulus stem from the difference of the fluctuation contributions to B.

4.5. Bulk and shear moduli in the fcc state

Data from the $N = 2048$-particle system, which is in the fluid and in the fcc state for densities $n < 0.96$ and $n > 0.97$, respectively, are presented in Figs. 8 and 9. In particular, the potential contribution p_{pot} to the pressure (open circles) and the bulk modulus B (filled circles) are displayed in Fig. 8 together with the values for the bulk modulus inferred from the ratio of the pressure and density differences (triangles). The two sets of data agree well also in the fcc state. Notice the strong variation of B in the vicinity of the fluid–solid phase transition. This is due to the large variations of the fluctuation contribution (46) to the bulk modulus.

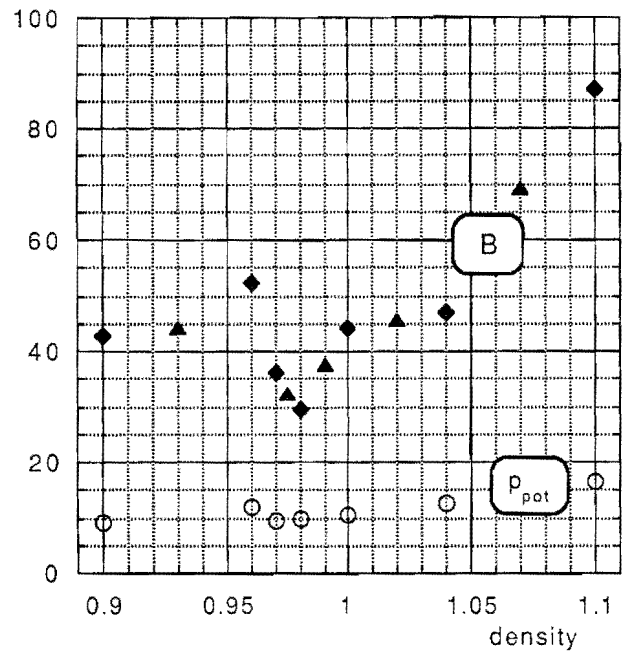

Fig. 8. The potential contribution p_{pot} (open circles) and the bulk modulus B as function of the density n for the $N=2048$ particle system, which is in the fluid and in the fcc state for $n \leqslant 0.96$ and $n \geqslant 0.97$, respectively. The filled diamonds show the values computed according to $B = B^{BG} + B^{flct}$ as given in the text; the triangles in between are the values inferred from the ratio of the pressure and density differences.

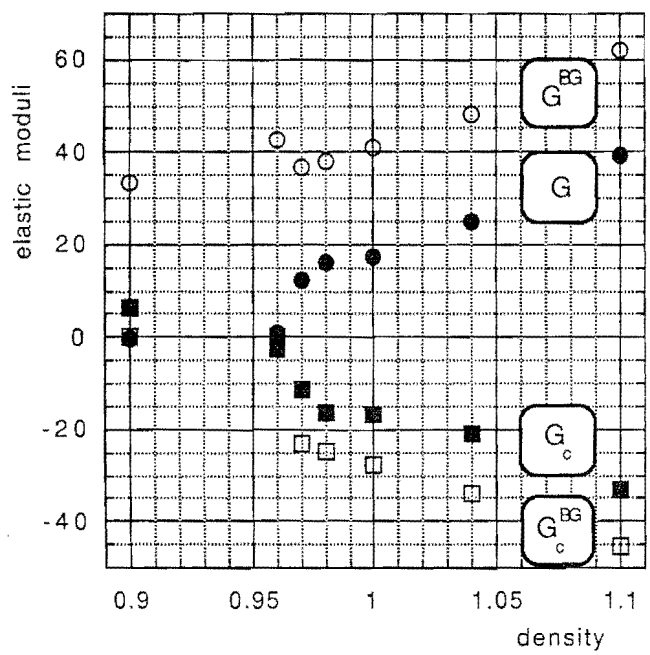

Fig. 9. The shear modulus G (circles) and the cubic modulus G_c (squares) as functions of the density n for the $N=2048$ particle system, which is in the fluid and in the fcc state for $n \leqslant 0.96$ and $n \geqslant 0.97$, respectively. The open symbols are for the Born–Green contributions. The filled symbols show the sum of the corresponding Born–Green and fluctuation contributions.

The elastic moduli G (filled circles) and G_c (filled squares) are displayed in Fig. 9 together with the corresponding Born–Green contributions (open symbols). Whereas G^{BG} just shows a slight discontinuity at the fluid–solid-phase transition, the shear modulus G and the Born–Green part of the cubic modulus G_c are zero and non-zero in the fluid and the solid states, respectively. Of course, the total modulus G_c should also vanish in the isotropic fluid state. The fact that this quantity does not vanish, e.g. for $n=0.9$, is due to the larger uncertainty involved in the computation of the fluctuation contribution. Compared to the Born–Green contributions, longer time averages are needed. As a side remark, it is mentioned that the cubic modulus G_c is not only negative in the fcc state but also in bcc state whereas it is positive in a simple cubic crystal. In all cases, the x-, y- and z-directions are chosen to be parallel to the cubic axes. This is easy when the simulation starts with an initial crystalline state. When the solid phase is approached by increasing the density or by lowering the temperature from an isotropic fluid state, the directions of the crystalline axes are not known beforehand. Then all components of the shear modulus tensor have to be computed. Furthermore, poly-crystallinity may occur. For this reason, the shear modulus G is the most appropriate indicator of solidification. The Voigt elastic moduli c_{11}, c_{12} and c_{44} can be obtained from the values of B, G, and G_c according to (39). The shear modulus c_{44} as well as $\tilde{c}_{44}=(c_{11}-c_{12})/2$ vanish discontinuously at the melting transition. This is in contradiction to a conjecture put forward by Born [1] but in accordance with the observations made previously in Monte Carlo simulations for Lennard–Jones solids [20]. Notice that the effect of a finite pressure is taken into account in the definitions of the elastic coefficients used here; cf. (18) and (23).

In summary, one infers from Fig. 9 that the orientationally averaged shear modulus is a good indicator for the fluid–solid-phase transition. The loss of cubic symmetry in melting a crystalline state is most clearly revealed by the vanishing of G_c^{BG}.

5. Concluding remarks

Expressions for the elastic modulus tensor and the Voigt elastic moduli have been presented. For particles interacting with a central potential, molecular dynamics simulations for a model system yielded numerical data for the shear and bulk moduli and provided a test of various relations derived. The general expressions given, however, also apply to fluids of non-spherical particles as occurring in molecular liquids, in liquid crystals and in molecular solids. In particular, it is of interest to extend the present approach to nematic and smectic liquid crystals, where symmetry considerations for the elastic modulus tensor can follow those known for the viscosity tensor [19]. Furthermore, it should be possible to treat the Frank elasticity of nematic liquid crystals in a similar manner.

Acknowledgements

This work has been performed under the auspices of the Sonderforschungsbereich 335 "Anisotrope Fluide". Financial support by the Deutsche Forschungsgemeinschaft is gratefully acknowledged.

References

[1] M. Born, J. Chem. Phys. 7 (1939) 591; Proc. Camb. Phil. Soc. 36 (1940) 160; M. Born and K. Huang, Dynamical Theory of Crystal Lattices (Oxford University Press, Oxford, 1954); H.S. Green, The Molecular Theory of Fluids (North-Holland, Amsterdam, 1952); M.S. Green, J. Chem. Phys. 22 (1954) 398.
[2] R. Zwanzig and R.D. Mountain, J. Chem. Phys. 43 (1965).
[3] S. Hess, Int. J. Thermophys. 6 (1985) 657.
[4] D.R. Squire, A.C. Holt and W.G. Hoover, Physica 42 (1969) 388.
[5] W.G. Hoover, A.C. Holt and D.R. Squire, Physica 44 (1969) 437.
[6] M. Schoen, S. Hess and D.J. Diestler, Phys. Rev. 52 (1995) 2587.
[7] F.C. von der Lage and H.A. Bethe, Phys. Rev. 71 (1947) 612; A. Hüller and J.W. Kane, J. Chem. Phys. 61 (1974) 3599.
[8] S. Hess, Z. Naturforsch. 35a (1980) 69; Physica A 127 (1984) 509; N. Herdegen and S. Hess, Physica A 138 (1986) 382.
[9] W.G. Hoover, Molecular Dynamics (Springer, Berlin, 1986); Computational Statistical Mechanics (Elsevier, Amsterdam, 1991); Physica A 194 (1993) 450.
[10] M.P. Allen and D.J. Tildesley, Computer Simulation of Liquids (Clarendon, Oxford, 1987).
[11] D.J. Evans and G.P. Morris, Statistical Mechanics of Nonequilibrium Liquids (Academic Press, London, 1990).
[12] S. Hess and W. Loose, Molecular dynamics: test of microscopic models for the material properties of matter, in: Constitutive Laws and Microstructure, eds. D. Axelrad and W. Muschik (Springer, Berlin, 1988) p. 92; S. Hess, D. Baalss, O. Hess, W. Loose, J.F. Schwarzl, U. Stottut and T. Weider, in: Continuum Models and Discrete Systems, Vol. 1, ed. G.A. Maugin (Longman, Essex, 1990) pp. 18–30; T. Weider, U. Stottut, W. Loose and S. Hess, Physica A 174 (1991) 1.
[13] S. Hess, Rheology and shear induced structure of fluids, in: Rheological Modelling: Thermodynamical and Statistical Approaches, eds. J. Casas-Vázques and D. Jou, Lecture Notes in Physics, Vol. 381 (Springer, Berlin, 1991) pp. 51–73; Physikal. Blätter 44 (1988) 325.
[14] S. Hess, M. Kröger, W. Loose, C. Pereira Borgmeyer, R. Schramek, H. Voigt and T. Weider, Simple and complex fluids under shear, in: Monte Carlo and Molecular Dynamics of Condensed Matter Systems, eds. K. Binder and G. Ciccotti, IPS Conf. Proc., Vol. 49, Bologna (1996) pp. 825–841; S. Hess, Constraints in molecular dynamics, nonequilibrium processes in fluids via computer simulations, in: Computational Physics, eds. K.H. Hoffmann and M. Schreiber (Springer, Berlin, 1996) pp. 268–293.
[15] R. Haberlandt, S. Fritzsche, G. Peinel und K. Heinzinger, Molekular-Dynamik (Vieweg, Braunschweig, 1995).
[16] B.J. Alder, W.G. Hoover and D.A. Young, J. Chem. Phys. 49 (1968) 3688.
[17] H.A. Posch, W.G. Hoover and O. Kum, Phys. Rev. 52 (1995) 1711, 4899; W.G. Hoover and S. Hess, Physica A 231 (1996) 425.
[18] H.M. Lindsay and P.M. Chaikin, J. Phys. 46 (1988) C3-269.
[19] S. Hess, J. Non-Equilibr. Thermodyn. 11 (1986) 176.
[20] A.C. Holt, W.G. Hoover, S.G. Gray and D.R. Shortle, Physica 49 (1970) 61.